Cyber-physical energy-saving control for hybrid aircraft-towing tractor based on online swarm intelligent programming

Zhou, Quan; Zhang, Yunfan; Li, Ziyang; Li, Ji; Xu, Hongming; Olatunbosun, Oluremi

DOI:
10.1109/TII.2017.2781230

Document Version
Peer reviewed version

Citation for published version (Harvard):
Zhou, Q, Zhang, Y, Li, Z, Li, J, Xu, H & Olatunbosun, O 2018, 'Cyber-physical energy-saving control for hybrid aircraft-towing tractor based on online swarm intelligent programming', *IEEE Transactions on Industrial Informatics*, vol. 14, no. 9, pp. 4149-4158. https://doi.org/10.1109/TII.2017.2781230

Cyber-Physical Energy-Saving Control for Hybrid Aircraft-Towing Tractor based on Online Swarm Intelligent Programming

Quan Zhou, *Member*, *IEEE*, Yunfan Zhang, Ziyang Li, Ji Li, Hongming Xu, Oluremi Olatunbosun

***Abstract*—This paper researches on a cyber-physical energy-saving control framework for a plug-in hybrid aircraft-towing tractor, in which, an online optimization methodology named the Online Swarm Intelligent Programming (OSIP) is proposed. The new methodology obtains real-time optimal control signals from the V2X network and the widely-used Charge Depleting/Charge Sustaining (CD/CS) strategy is upgraded to a more adaptive and intelligent level. The energy-flow of the hybrid aircraft-towing tractor with connectivity is firstly analysed and modelled for OSIP. The optimal control problem is then formulated as an online integer optimization and the OSIP algorithm based on Chaos-enhanced Accelerated Swarm Optimization (CAPSO) is developed to minimize the powertrain power loss in real-time. Finally, the advantages of the new energy management system are demonstrated and evaluated by hardware-in-the-loop testing. The results show that up to 17% fuel and 13% total energy loss can be saved via the proposed cyber-physical control.**

***Index Terms*—Cyber Physical Control, Plug-in Hybrid Tractor, Real-time Integer Optimization, Chaos-enhanced Accelerated Particle Swarm Optimization, Hardware-In-the-Loop Test.**

I. Introduction

NOWADAYS, the increasingly stringent emission and fuel consumption regulations are forcing the motor industry to move to vehicle hybridization. Advanced hybrid vehicle system requires increasing number of components working cooperatively to optimize the vehicle performance [1]–[7]. Consequently, powerful and reliable supervisor controllers are needed to ensure all the hybrid components are really working properly. The energy management controller is one of the vital supervisor controllers in the hybrid electric vehicle, which supervises and controls the sub-system controllers, such as engine controller, motor controller, battery management system, etc.

For real-time energy management of plug-in HEVs, the "Charge-Depleting/Charge-Sustaining (CD/CS)" strategy is the most representative method [8], [9], which switches the hybrid system working mode between CD and CS based on the predefined rules. In the CD mode, the alternative power unit (APU) does not generate any power for battery package (BP) charging; in the CS mode, the APU generates the power to maintain the BP's SoC within a proper range. Although the CD/CS strategy has been implemented to mass-produced HEV products, its limitation is still obvious because that it is not a kind of optimal control method and cannot be adapted to all possible scenarios.

Recently, cyber-physical control emerges as a new concept of adaptive real-time control, which works on a distributed, networked and intelligent system that fuses computational processes (cyber) with the physical world [10]. With the help of vehicle-to-vehicle (V2V) and vehicle-to-infantry (V2I) communication, sufficient data is available for environment perception and accurate predictive modelling [11]. Furthermore, the Internet of vehicle (IoV) also makes it possible to perform intelligent algorithms in the cloud and controls the vehicles via cyber-physical framework [12]. Therefore, the IoV concept inspires the idea of upgrading the existing rule-based energy management system into an adapted and intelligent system for the connected special-utility vehicles including aircraft-towing tractors.

As a preparation of cyber-physical control for connected HEVs, model predictive control (MPC) framework is a competitive candidate and many researches on MPC for non-cyber-physical platforms can be found in literatures [13]–[17]. The MPC obtains the optimal control trajectory that maximizes the system performance in the prediction horizon subjected to constrains [18]. An appropriate solver should be chosen in order to solve the optimization problems at each time interval in the MPC. Generally, MPCs are solved by gradient-based Newton's methods. For example, the nonlinear MPC is solved by sequential quadratic programming (SQP) [11]; the mixed-integer optimization problems in hybrid MPC is solved by the hybrid toolbox in MATLAB[19]; MATLAB command 'quadprog' [1], 'CVXGEN' [20] and 'qpOASES' [21] are for quadratic programming (QP) of linear constrained MPCs. However, only linear MPCs have been realized the feature of real-time implementation, running nonlinear MPC for HEV energy management in real-time controllers has yet to be demonstrated [14].

Particle swarm optimization (PSO) algorithm is a potential candidate for real-time NMPC solving [22], since it works with fewer tuning parameters and less computational effort. PSO also has the capability of dealing with integer variables and it has been successfully applied in hybrid electric vehicle offline optimization [23]–[26]. Furthermore, the PSO's convergence speed and the capability of finding the real global optima can be further optimized by upgrading the standard PSO into Chaos-enhanced Accelerated Particle Swarm Optimization (CAPSO) algorithm [27]. The work of the authors has proved

Manuscript received 22nd September 2017; revised 15th November 2017; accepted 1st December 2017. This work was supported by Innovate UK (Grant 102253).

Q. Zhou, Y. Zhang, Z. Li, J. Li, H. Xu and O. Olatunbosun are with Department of Mechanical Engineering, the University of Birmingham, Birmingham, B15 2TT, UK. (email address: q.zhou@pgr.bham.ac.uk, yxz278@bham.ac.uk z.li.6@pgr.bham.ac.uk, jxl592@bham.ac.uk, h.m.xu@bham.ac.uk, o.a.olatunbosun@bham.ac.uk)

(Corresponding Author: Professor Hongming Xu, h.m.xu@bham.ac.uk)

that CAPSO outperforms the standard PSO in solving offline integer nonlinear optimizations [28].

To develop a powerful and implementable real-time control strategy for the optimal control of connected HEVs, this paper proposes an Online Swarm Intelligent Programming (OSIP) methodology based on CAPSO algorithm. The new methodology obtains real-time optimal control signals from the V2X network and the widely-used CD/CS strategy is upgraded to a more adaptive and intelligent level. The work is carried out as follows: (1) a cyber-physical framework for hybrid aircraft towing tractor energy management is developed and the energy flow of the system is modelled for real-time OSIP. (2) The real-time energy management is formulated as an online nonlinear integer optimization and the CAPSO algorithm for OSIP is developed to solve the nonlinear integer optimization. (3) The energy management by OSIP is implemented into a real-time controller, and the advantages of the proposed method are further demonstrated with hardware-in-the-loop (HIL) test.

The rest of this paper is structured as follows: section II introduces the cyber-physical framework and the vehicle system models for real-time control purpose. In Section III, the local control strategy and online swarm intelligent programming are provided in detail. Section IV presents the experimental set-up for real-time implementation, validation and evaluation. The performance of the proposed energy management system is evaluated by convergence analysis, computational afford analysis, hardware-in-the-loop test and the robustness & repeatability in section V. Section VI summarises the conclusions.

II. System Configuration and Modelling

The traffic in the airport is a complex and interconnected system, which includes aircrafts, towing tractors and ground support vehicles. The V2X network (with vehicles, aircrafts and infrastructures connected) carries out predictive modelling and control optimisation of the system using advanced algorithms based on collected data and powerful cloud computing facilities. This will save energy by organizing the traffic and individual vehicle operation. Aircraft towing is one of the most typical individual vehicle operation scenario. Fig. 1. shows the aircraft towing scenario studied in this paper, which consists of the aircraft towing tractor, the aircraft, the airport control, and V2V & V2I communications. The control 1) receives the tractor and aircraft's real-time state signal via V2I network; 2) operates programming of optimal future control command for energy saving in the cloud; 3) sends the command signal back to the vehicle controller via V2I network. This framework with advanced intelligent algorithms enables the real-time optimal control of energy flow for energy saving which was previously limited by the performance of local vehicle controller.

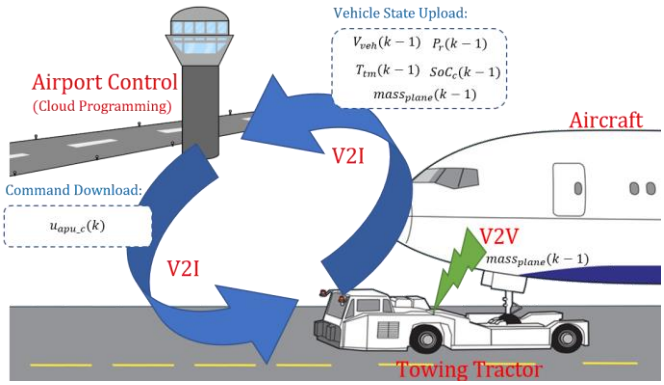

Fig. 1. Aircraft towing scenario with V2V/V2I communication

The main components of the hybrid tractor include a 245-kW traction motor, an 86.2kW alternative power unit, and a battery package with 8200 NCR-18650 series lithium-ion cells in Fig. 2. The main states of the tractor and aircraft considered within the framework are vehicle and aircraft speed, aircraft mass, tractor power requirement and battery pack's SoC. The command signal downloaded from the server controller is modified power command of the alternative power unit.

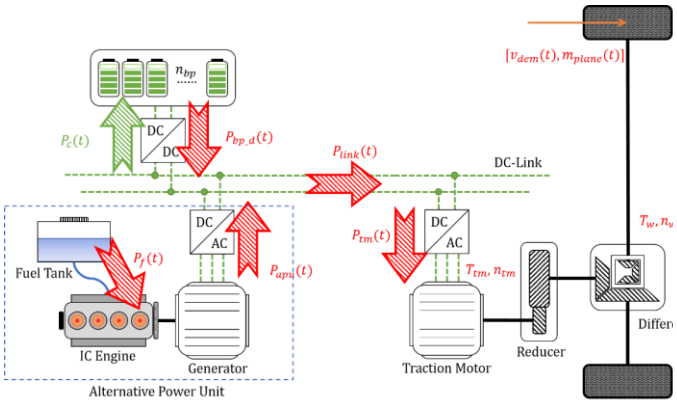

Fig. 2. System configuration and power-flow

TABLE I
Vehicle Profile

Specification	Value
Vehicle mass	16 tonnes
Front area	6.8 m^2
Drag coefficient	0.8
Friction coefficient	0.02
Fixed gear ratio	25

A. Hybrid Electric Vehicle Power-flow

The power-flow of the vehicle system obeys:

$$P_{link}(t) = P_{apu}(t) + P_{bp\_d}(t) - P_c(t) \quad (1)$$

where $P_{apu}(t)$ is the output power provided by the APU, $P_{bp\_d}(t)$ is the discharge power of the BP, $P_c(t)$ is the BP's charge power, and $P_{link}(t)$ is the power of the DC-link, and obeys:

$$P_{link}(t) = P_{tm}(t) + P_{loss,tm}(t) \quad (2)$$

where $P_{loss,tm}(t)$ is the power loss in the traction motor, and $P_{tm}(t)$ is the power for driving the vehicle. The main parameters for vehicle dynamic calculation are listed in Table I.

B. Real-time Component Efficiency Modelling

To predict the powertrain performance online, the main powertrain components are modelled in real-time by numerical method using the original testing data from the OEMs. The model is verified by comparing the modelling results compared with the original testing data in Fig. 3. The details in the components modelling are described as follows:

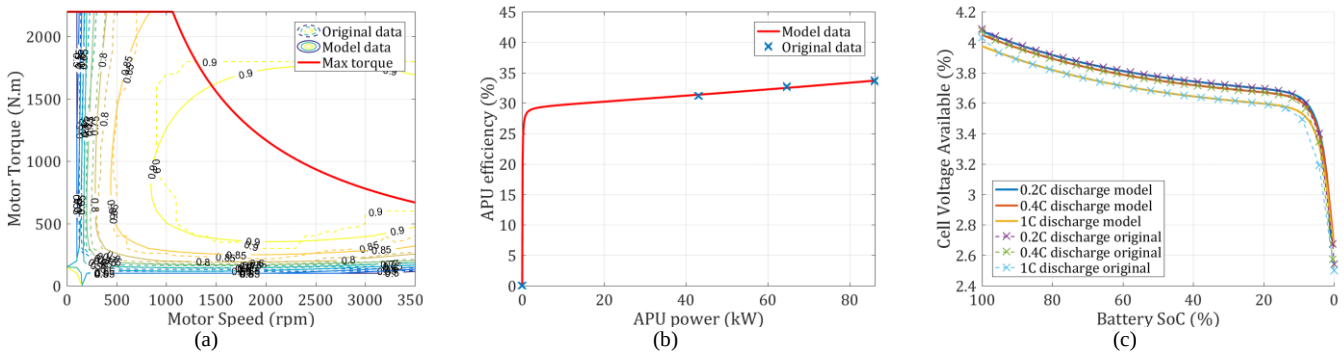

Fig. 3. Validated control-orientated model with data of the powertrain components: (a) electric motor efficiency, (b) alternative power unit efficiency, (c) battery cell OCV

1) Traction motor

The selected traction motor is a heavy duty electric motor (type: LSM280A HV-2700) provided by TM4 electrodynamic system Ltd. The motor specification is listed in Table II. As a low speed vehicle, it is not cost-efficient to use a regenerative braking system. Therefore, the traction motor is only working in traction mode. The traction motor's real-time efficiency is described by:

$$\eta_{tm}(t) = \frac{P_{tm}(T_{tm}(t),n_{tm}(t))}{P_{tm}(T_{tm}(t),n_{tm}(t))+P_{loss,tm}(T_{tm}(t),n_{tm}(t))} \quad (3)$$

where the power for traction $P_{tm}$is a function of traction torque T_{tm} and rotational speed n_{tm}. The motor power loss $P_{loss,tm}$is also a function of motor torque T_{tm} and motor speed n_{tm} and $P_{loss,tm}$in this paper is formed as a quadratic function [2] using the data provided by the motor supplier.

TABLE II
TRACTION MOTOR SPECIFICATION

SPECIFICATION	VALUE
Nominal power	245 kW
Nominal torque	2200 Nm
Max. operation speed	3375 rpm
Inverter	CO300HV
Peak efficiency	95%

2) Alternative power unit

An 86.2 kW alternative power unit (APU) produced by JCB is selected. The APU is powered by a 4.4L diesel engine, and generates electric power with a 3-phase AC generator. Main technical parameters of the selected APU are listed in Table III. The APU's real-time efficiency is:

$$\eta_{f2e}(t) = \frac{P_{apu}(t)}{P_{fuel}(P_{apu}(t))} \quad (4)$$

where, P_{apu} is the real-time APU output power to the DC-link controlled by the energy management system. The real-time equivalent fuel consumption power is also mapped as a quadratic function of P_{apu} [2], and main parameters of function $P_{fuel}$are calibrated by calculating the real-time $P_{fuel}(t)$ with the measured real-time fuel consumption rate $\dot{v}_f(t)$ in L/h, the density of the fuel ρ_f, and the heat value of the fuel H_f.

TABLE III
ALTERNATIVE POWER UNIT SPECIFICATION

SPECIFICATION	VALUE
Max. primer power	86.20 kW
Fuel type	diesel
Max. operation speed	3375 rpm
50% load fuel rate	13.00L/h
75% load fuel rate	18.60L/h
100% load fuel rate	24.10L/h
Fuel tank capacity	285L

3) Battery package

The battery pack (BP) is made up with the battery cell type NCR-18650 series provided by Panasonic Automotive & Industrial System Ltd. The voltage of battery cells ranges from 2.5 V to 4.2 V, and the nominal battery voltage is 3.7V. The battery cell's rated capacity is 2450mAh. The battery pack is made up of 8200 battery cells. For the control-oriented battery model, a simple resistive circuit is chosen[29]. The BP's real-time efficiency model is modelled as:

$$\eta_{bp}(t) = \frac{Num_{bc}\cdot V_{oc}(SoC)\cdot \mathrm{I_{bc}}(t) - Num_{bc}\cdot R_{loss}(SoC)\cdot I_{bc}(t)^2}{Num_{bc}\cdot V_{oc}(SoC)\cdot \mathrm{I_{bc}}(t)} \quad (5)$$

where Num_{bc} is the total number of battery cells in the BP; $V_{oc}$is the open circuit voltage of a single battery cell; $R_{loss}$is the internal resistance in the equivalent battery circuit; I_{bc} is the battery cell current. The open circuit voltage V_{oc} and the battery's internal resistance R_{loss} are modelled as SoC dependent exponential functions using the original data from the battery OEM. The model for the open circuit voltage V_{oc} and the battery internal resistance R_{loss} are [30]:

$$\begin{cases} V_{oc}(SoC) = c_4 \cdot e^{c_5 \cdot SoC} + c_3 \cdot SoC^3 + c_2 \cdot SoC^2 + c_1 \cdot SoC + c_0 \\ R_{loss}(SoC,\ I_{bc}) = \dfrac{SoC}{c_6(I_{bc}) + c_7(I_{bc}) \cdot SoC} \end{cases} \quad (6)$$

where, c_i $(i = 0,1,\dots 7)$ are the model parameters, in which, c_1 to c_4 are constant, and c_6 and c_7 are I_{bp} dependent polynomial functions. All the model parameters are determined by curve fitting using the test data.

C. V2I and V2V communication

With the proposed cyber-physical system, tractors will be connected with the remote serve in the airport control via the road side units (RSUs) near the tractors' working area. The remote serve will enable the real-time optimization based on cloud computing via advanced online programming algorithms, Through the V2I communication, the online swarm-intelligent programming will be available working on the remote serve located in the airport control and will send the optimal control command to the local vehicle controller. Subsequently, the V2V communication between the tractor and aircraft will enable the basic control function of the tractor controller.

III. Real-time Optimal Energy-flow Control

The real-time optimal control system includes the local energy-flow control and the cloud-based Online Swam Intelligent Programming (OSIP) in Fig.4. The local control performs on the on-boarded vehicle controller and the OSIP operates on the connected server. As the energy management system mainly considers the energy split and management, one second is chosen according to [15] as the sampling time, which is approved to be able to track the system dynamics while reserving enough time slot for algorithm computing. The mechanism of local energy-flow control and OSIP is as follows:

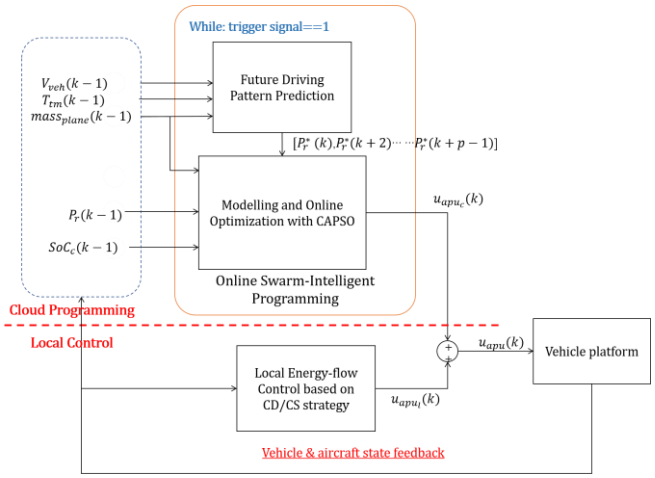

Fig. 4. Real-time optimal energy flow control based on online swarm intelligent programming

A. Local Energy-flow Control

In the local vehicle controller, the widely-used CD/CS strategy [10,11,14] is applied for the energy flow control. The CD/CS strategy defines the APU control input u_{apu_c} as a precise exponential function of the BP's SoC [31]. The control input of the APUu_{apu_l} has a resolution of 0.05, therefore the CD/CS strategy is modified as:

$$u_{apu\_l}(SoC) = \begin{cases} 0 & SoC \in (0.8,1] \\ round(20 \cdot e^{(-\frac{(SoC-0.2)^2}{2\sigma^2})})/20 & SoC \in [0.2,0.8] \\ 1 & SoC \in [0,0.2) \end{cases} \quad (7)$$

where SoC is BP's state of charge, $\sigma = 0.1$ is the time constant.

B. Online Swarm Intelligent Programming

The proposed OSIP is an online real-time optimization performing on the cyber-physical system, which upgrades the local CD/CS strategy into an advanced adaptive control with intelligent algorithm. The OSIP firstly formulates the energy management as an integer nonlinear optimization problem based on vehicle performance prediction using the data from V2I communication. Then, the integer nonlinear optimization is solved in real-time via a specially designed Chaos-enhanced Accelerated Particle Swarm Optimization (CAPSO) algorithm. The optimization result is sent back to local controller via I2V communication. The OSIP is developed as follows:

1) Objectives and constrains

To minimize the energy loss over each predictive horizon, the objective function for optimal control at k th ($k = 0,1,2,3 \ldots$) time interval is represented by:

$$J_k = \sum_{t=k}^{k+p-1} x_{apu}(t) \cdot \Delta t + \sum_{t=k}^{k+p-1} x_{batt}(t) \cdot \Delta t \quad (8)$$

where p is the size of predictive horizon; J is the objective function depending on the cloud computed APU's command modification signal $u_{apu\_c}(t)$; The state variable of the APU $x_{apu}(t)$ and BP $x_{bp}(t)$ are their power loss rate at each sampling time instant:

$$\begin{cases} x_{apu}(t) = u_{apu}(t) \cdot P_{apu\_max} \cdot (1 - \eta_{f2e}(\cdot)) \\ x_{batt}(t) = (\frac{1}{2}\left(V_{oc}(SoC) - \sqrt{V_{oc}(SoC)^2 - \frac{4R_{loss}(\cdot)u_{batt}(t) \cdot P_{bp\_max}}{Num_{bc}}}\right))^2 \cdot \frac{Num_{bc}}{R_{loss}(\cdot)} \end{cases} \quad (9)$$

where P_{apu_max} and P_{bp_max} are the APU's maximum power generation and battery pack's maximum power generation respectively; Num_{bc} is the number of battery cells in the BP; η_{f2e} is the APU's fuel to electric efficiency, calculated by equation (5); R_{loss} is the battery cell's internal resistance calculated by equation (8); u_{apu} is the final control command summed with the local APU command u_{apu_l} and the cloud computed command modification u_{apu_c}. The battery control command u_{batt} is calculated by:

$$u_{batt}(t) = \frac{(P_r(t) - u_{apu}(t) \cdot P_{apu\_max})}{P_{batt\_max}}. \quad (10)$$

where $P_r(t)$ is the predicted vehicle power requirement which will be discussed in the following section. The APU's control output has a resolution of 0.05, therefore, the APU's control output u_{apu} should be constrained as:

$$\begin{cases} 0 \le u_{apu}(t) \le 1 \\ u_{apu}(t) = 0.05 \cdot gain(t) \ (gain(t) \ is \ an \ integer) \end{cases} \quad (11)$$

To ensure the battery package is performing in proper condition and protect the BP from over charge or over discharge, the battery's state of charge should obey[8]:

$$0.2 \le SoC(t) \le 0.8 \quad (12)$$

The optimal energy-flow control problem at time interval k can be mathematically formulated in equation (13).

$$\min_{u_{apu\_c}} J_k = \sum_{t=k}^{k+p-1} x_{apu}(t) \cdot \Delta t + \sum_{t=k}^{k+p-1} x_{batt}(t) \cdot \Delta t$$
$$s.t. \begin{cases} x_{apu}(t) = u_{apu}(t) \cdot P_{apu\_max} \cdot (1 - \eta_{f2e}(\cdot)) \\ x_{batt}(t) = (\frac{1}{2}\left(\sqrt{V_{oc}(SoC) - \frac{4R_{loss}(\cdot)u_{batt}(t) \cdot P_{bp\_max}}{Num_{bc}}}\right))^2 \cdot \frac{Num_{bc}}{R_{loss}(\cdot)} \\ u_{batt}(t) \cdot = \frac{(P_r(t) - u_{apu}(t) \cdot P_{apu\_max})}{P_{batt\_max}} \\ u_{apu}(t) = u_{apu\_c}(t) + u_{apu\_l}(t) \\ 0 \le u_{apu\_c}(t) + u_{apu\_l}(t) \le 1 \\ u_{apu\_c}(t) = 0.05 \cdot gain(t) \ (gain(t) \ is \ an \ integer) \\ 0.2 \le SoC \le 0.8 \end{cases} \quad (13)$$

2) Future power demand prediction

To simplify the modelling of future power demand, the driver torque demand is assumed to be exponentially varying over the predictive horizon based on empirical formula [14], [18], [32];

therefore, the motor torque demand T_{tm} is predicted as an exponential function over the prediction horizon as in:

$$T_{tm}(k+i-1|k) = T_{tm}(k+i-2|k) \cdot e^{(-\frac{i\tau_s}{\tau_d})} \quad (i = 1, 2 \dots p) \tag{14}$$

where, $T_{tm}(k-1|k)$ is the known motor torque value measured at the end of the last time interval, $T_{tm}(k|k), T_{tm}(k+1|k), \dots T_{tm}(k+p-1|k)$ are the predicted motor torque over the prediction horizon p, $\tau_s = 1s$ is the sample time and τ_d determines the decay rate. As the airplane mass is much larger than the vehicle mass, the torque decay rate varies dramatically when pushing back different aircrafts, therefore, τ_d is redefined as a function of airplane mass in kilogram as:

$$\tau_d = \tau_0 \cdot mass_{plane} \tag{15}$$

where, $\tau_0 = 2.36 \times 10^{-3}$ is the unit decay rate which is tuned with the real driving cycle corresponding to the airplane mass $mass_{plane}$. When the torque requirement is available from equation (14) and (15), it is easy to predict the future power demand by using vehicle dynamics formulas in [16], [33].

3) Algorithm for online programming

Fig. 5. shows the core algorithm for OSIP in a single time instant. The algorithm is developed based on CAPSO, which has three main procedures, namely, initialization, main iteration, and optimal position retrieving. The details and principle of the CAPSO algorithm working procedure are discussed in the author's previous work in [27]. To solve the optimization problem in equation (13) online, the algorithm is customised and modified in the following aspects:

a) The definition of particle position:

At initialization procedure, the position of particles is defined as:

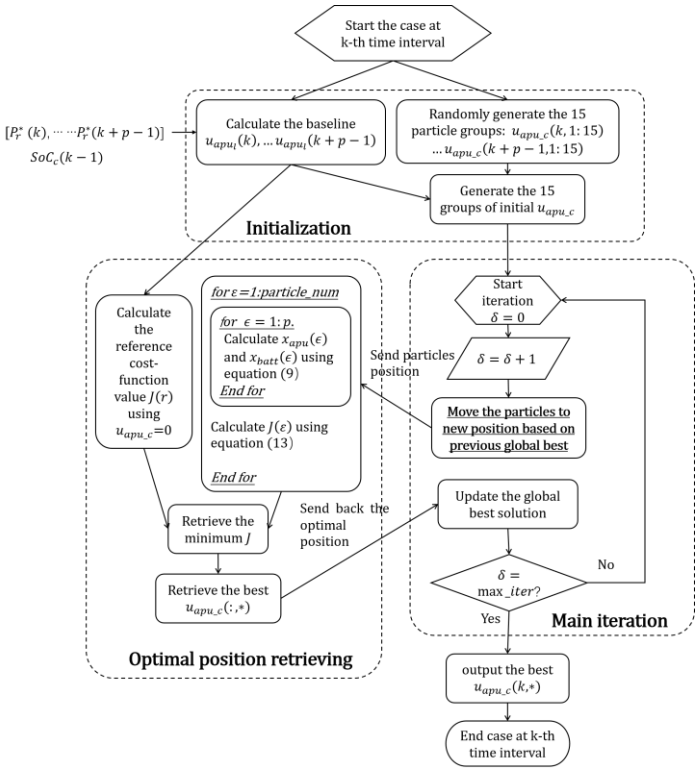

Fig. 5. Flow-chat of CAPSO algorithm for OSIP in a single time instant.

$$p_{\delta,\varepsilon} = U_{apu_t} \quad \delta \in [1, \max\_iter], \varepsilon \in [1, particle\_num] \tag{16}$$

where $U_{apu\_l} = [u_{apu\_l}(k|k), u_{apu\_l}(k+1|k), \dots, u_{apu\_l}(k+p-1|k)]$ is the could computed APU command modification vector over the predictive horizon p; δ is the index for number of iterations; ε is the index for each particle. To obtain sufficient adequate accuracy with the least computing effort, the value of maximum iteration $\max\_iter$ is 30 and the number of particles $particle\_num$ is 15 as [22]. The feasibility of the settings will be observed in section V-A.

b) Random number generation with specific resolution:

In main interaction procedure, the key step is move the particles to the new position, and the random number with resolution is required for moving particles. The random number generation with a resolution of 0.05 is modified from the standard Linear Congruential Generator (LCG):

$$\begin{cases} R_\epsilon = (a \cdot R_{\epsilon-1} + c) \, mod \, M \\ rnd(k+\epsilon-1) = round(20 \cdot \frac{R_\epsilon}{M})/20 \end{cases} \tag{17}$$

where multiplier a, additive constant c, and modulus M are integers. Equation (17) defines a series of random number with the initial seed R_0. The vector $\{rnd_{i,\epsilon}\ (\epsilon = 1,2, \dots p)\}$ is a random number sequence from 0 to 1, with resolution of 0.05. To maximise the pseudo-random number performance, the parameters of the LCG are [22]: R_0 =9, $a = 27$, $c = 0$, and $M = 2^{20}$.

c) Particle position updates:

In main interaction procedure, the position of particles updates as:

$$p_{\delta+1,\varepsilon} = res \cdot round\{(1-\beta) \cdot \frac{p_{\delta,\varepsilon}}{res} + \beta \cdot \frac{g_{\delta,*}}{res} + \gamma^\delta \cdot \zeta \cdot [\text{rand}(0,1) - 0.5]\} \tag{18}$$

where, $p_{\delta+1,\varepsilon}$ is the updated position, $p_{\delta,\varepsilon}$ is the particle's position of the present iteration, $g_{\delta,*}$ is the best position of the present iteration, δ is the iteration generation, ε is the particle's individual index, res = 0.05 is the variable resolution, $\gamma = 0.85$ is the convergence parameters of CAPSO, $\zeta = 80$ is the search area factor, and β is the attraction parameters of CAPSO. The previous study of the authors suggested that the CAPSO with logistic chaotic map is the best for integer optimization [28]. The attraction parameters β is mapped in logistic map as:

$$\beta_{\delta+1} = \alpha \cdot \beta_\delta \cdot (1 - \beta_\delta) \tag{19}$$

where, the initial value of $\beta_1 = 0.7$ and $\alpha = 4$ are used for the logistic chaotic map[28].

d) Final outputs:

When convergence has been achieved, the algorithm ends the main iteration and outputs the best position at the end iteration $g_{\max\_iter,*}$ as the global optimal solution. Then the first element of the control sequence $u(k) = (u_{apu\_c}(k|k))$ is the final output of the OSIP controller.

IV. Testing and Validation Set-up

A. Driving Cycles

The push back speed and load of the aircraft-towing tractor vary in real practice but currently there is no standard driving cycle for aircraft-towing tractor performance evaluation. In this work, four types of Push Back Driving Cycles (PBDCs) are proposed, based on the statistical data collected at London Heathrow airport [27]. A PBDC is made up from four typical modes, namely, heavy pushback, medium pushback, light pushback and solo run. Each mode includes the profile of vehicle speed and the push-back load (airplane mass). Table IV provides the profile of different modes. Four different PBDCs are made by arranging these modes in different combination, Fig.6 provides the cycle pattern of PBDC-I and the cycle profiles of PBDC-I to PBDC-IV are summarized in Table V.

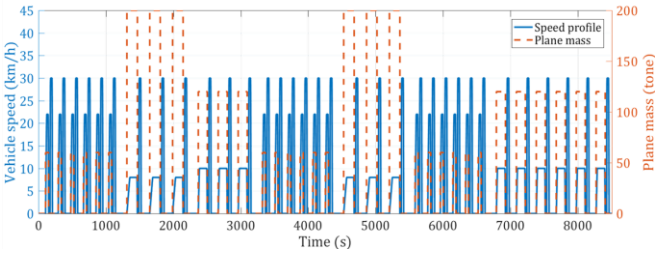

Fig. 6. The speed and plane mass profile of BPDC-I

TABLE IV
Cycle Mode Profile

Specification	Max. Speed	Airplane Mass	Acc. Time	Mode Length
Heavy (H)	8 km/h	200t	43s	155s
Medium (M)	10 km/h	120t	16s	133s
Light (L)	22 km/h	60t	17s	45s
Solo run (S)	30 km/h	0t	7s	35s

TABLE V
Push-back Driving Cycle Profile

Cycle Name	Cycle Mode Arrangement
PBDC-I	6 L&S+3 H&S+3 M&S+6 L&S+3 H&S+6L&S+6 M&S
PBDC-II	6 L&S+ 6 L&S+ 6 L&S+ 6 L&S+ 6 L&S
PBDC-III	3 M&S+ 3 M&S+ 3 M&S+ 3 M&S
PBDC-IV	2H&S+2 H&S+ 2 H&S+ 2 H&S+ 2 H&S+ 2 H&S

B. Hardware-In-the-Loop Test Set-up

The hardware in the loop test is used for testing the cyber-physical system's real-time performances. This paper uses the industrial level real-time testing facilities provided by ETAS Group [34]. The configuration of the HIL testing system and bench configuration are shown in Fig.7 and Fig.8 respectively. The cloud computing and V2I communication are performed in ETAS ES910, whose core components are a 1.5GHz processor with 4GB RAM and 1Gbps Ethernet communication. The control strategy and algorithm are programmed in host PC-1 and flashed to ES910 by ETAS INTECRIO. The DESK-LABCAR performs as the hybrid aircraft towing tractor with local controller and it communicates with the V2I interface (ES910) via CAN bus. The vehicle and local controller are modelled and complied in host PC-2 and downloaded to the DESK-LABCAR by ETAS Experiment Environment (EE) via Ethernet protocol. The vehicle performances are supervised by ETAS EE in host PC-2. The real-time models for the HIL test are developed using Simulink as in the authors' previous work [28], [35], and the models are verified by the test data from a prototype vehicle provided by the industrial partners [36].

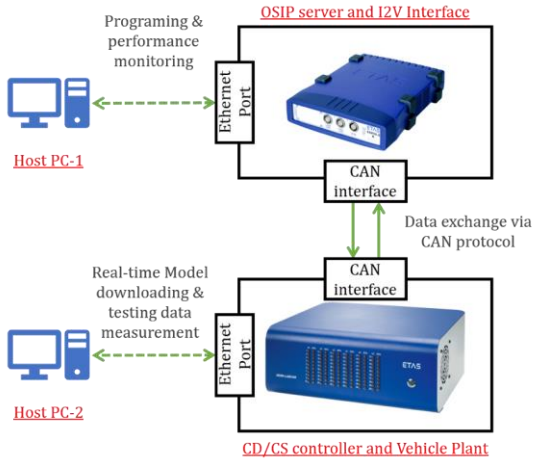

Fig. 7. Hardware-in-the-loop testing system

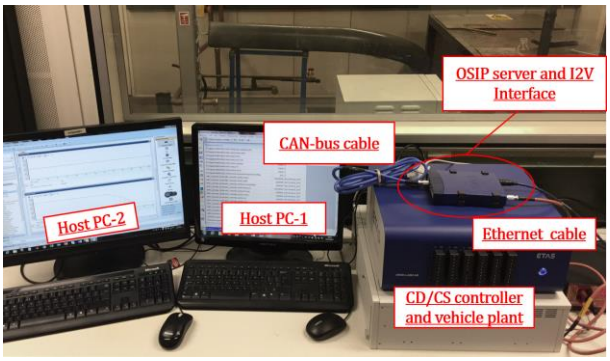

Fig. 8. Hardware-in-the-loop test bench

V. Results and Discussion

A. Optimization performance

TABLE VI shows that CAPSO algorithm for OSIP is able to find the global optimal solution identical to that obtained by MATLAB genetic algorithm (GA) toolbox but in a much faster process. The optimization process in four random selected time instants (500s, 1800s, 5050s and 6800s) is repeated using the two methods (i.e. CAPSO and GA) respectively for 20 times, and the optimal cost in the 20 trials is considered as the 'global optima'. Although the average cost function value is slightly lower with GA (<4%), the average computing time using GA for each time instant is more than 20s, whereas it is only less than 1s using CAPSO. Therefore, the advantage of CAPSO is

TABLE VI
Optimization Performance in Single Time Instant

Time instant	Method	Optimal cost	Average cost	Ave. Time
500s	GA	180678.53	194348.41	23.36s
	CAPSO	180678.53	200038.25	0.72s
1800s	GA	4787.43	5245.43	25.10s
	CAPSO	4787.43	5377.13	0.81s
5050s	GA	236331.20	244481.97	24.58s
	CAPSO	236331.20	252185.55	0.76s
6800s	GA	1653523.00	1662715.87	26.20s
	CAPSO	1653523.00	1687830.51	0.83s

outstanding because this fast response is extremely important for real time control.

B. Computational effort

The computational cost is a natural concern for real-time implementation and the prediction horizon size is the most concerned factor which affects the computational cost [11]. The computational cost of the proposed method with respective size of predictive horizon p is hereby investigated. The optimization problem is solved by the ETAS ES910 real-time controller. The average computational cost per time step including the data communication is shown in Fig.9. It indicates that while the augmented prediction horizon size p leads to increased computational load, prediction horizon size p being less than 36s can make the controller implementable in real-time, as the computing time is less than the sampling time of 1 second. The macro performance of the proposed method will be discussed in the following sections.

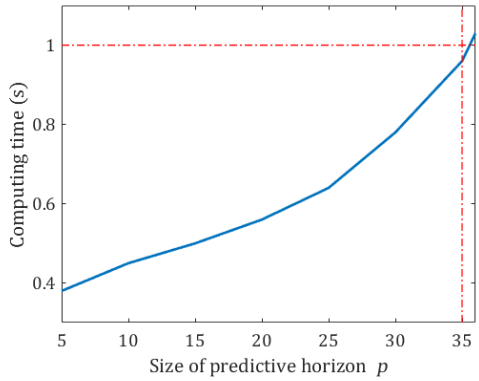

Fig. 9 Average computation time per step in PBDC-I

C. Vehicle system performance in real-time

The real-time performance of the connected system is evaluated and compared with the system using local control only. Different battery initially SoC values of 80% and 20% are investigated respectively in Fig.10 and Fig.11. The proposed control method can maintain the HEV's components working within the proper range in real-time. Fig.10 shows the HIL test result in PBDC-I assuming the battery is initially in full charge. In this condition, the connected system can save more energy than the one with local control only. Fig. 11 shows the HIL test result in PBDC-I assuming the battery initial SoC is low due to some unknown error. The connected system can work properly and also outperform the one without OISP.

D. Robustness and repeatability

The working condition varies among different scenarios; therefore, the test of robustness and repeatability is needed. The HEV systems in four PBDCs with different initial BP SoC values (80%, 50% and 20%) are evaluated, and the test results are given in Table VII. The results indicate that in all the scenarios under investigation, the proposed method outperforms the method with local control only in energy saving. The proposed method can reduce up to 17.17% fuel consumption and 13.06% of total energy loss. The highest fuel consumption reducing rate and highest energy saving rate are obtained over PBDC-III with the initial SoC of 80%.

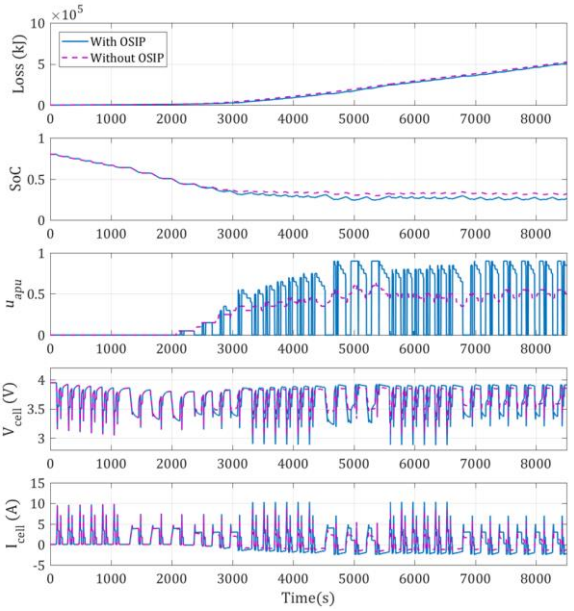

Fig.10 Real-time performance in PBDC-I when initial battery SoC=80%

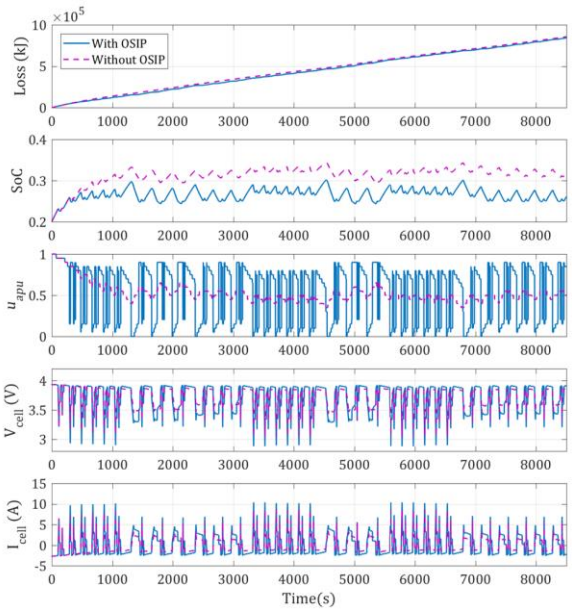

Fig.11 Real-time performance in PBDC-I when initial battery SoC=20%

VI. CONCLUSION

An online swam intelligent programming (OSIP) method for energy management of a connected plug-in hybrid aircraft-towing tractor has been studied. The vehicle performance with the proposed OSIP is evaluated by optimization performance analysis, computational effort analysis, HIL test, and robustness & repeatability test. The conclusions drawn from the investigation are as follows:

1. The proposed OSIP based on CAPSO algorithm has the capacity of finding global optima with much faster computing speed comparing with GA.
2. The OSIP can optimize the vehicle performance in real-

TABLE VII
VEHICLE PERFORMANCE OVER DIFFERENT SCENARIOS

DRIVING CYCLE	INITIAL SOC	CONTROL METHOD	TOTAL POWER LOSS(KJ)	SAVINGS	FUEL CONSUMPTION (L)	SAVINGS
BPDC-I	0.8	CD/CS	5.2614×10^5	-	16.53	-
	0.8	OSIP	5.0909×10^5	3.24%	15.76	4.59%
	0.5	CD/CS	6.9497×10^5	-	22.27	-
	0.5	OSIP	6.8200×10^5	1.87%	21.60	3.01%
	0.2	CD/CS	8.5618×10^5	-	27.79	-
	0.2	OSIP	8.4293×10^5	1.55%	27.11	2.45%
BPDC-II	0.8	CD/CS	1.3877×10^5	-	3.94	-
	0.8	OSIP	1.3171×10^5	5.09%	3.64	7.67%
	0.5	CD/CS	3.1002×10^5	-	15.31	-
	0.5	OSIP	3.0797×10^5	0.66%	14.85	2.06%
	0.2	CD/CS	4.7437×10^5	-	15.31	-
	0.2	OSIP	4.6738×10^5	1.47%	14.84	3.04%
BPDC-III	0.8	CD/CS	0.9516×10^5	-	2.73	-
	0.8	OSIP	0.8273×10^5	13.06%	2.26	17.17%
	0.5	CD/CS	2.6182×10^5	-	8.37	-
	0.5	OSIP	2.4203×10^5	7.59%	7.59	9.30%
	0.2	CD/CS	4.2393×10^5	-	13.91	-
	0.2	OSIP	4.0317×10^5	4.89%	13.11	5.75%
BPDC-IV	0.8	CD/CS	1.9791×10^5	-	5.98	-
	0.8	OSIP	1.8468×10^5	6.70%	5.46	8.67%
	0.5	CD/CS	3.0593×10^5	-	9.70	-
	0.5	OSIP	2.9470×10^5	3.67%	9.23	4.79%
	0.2	CD/CS	4.1117×10^5	-	13.35	-
	0.2	OSIP	3.9978×10^5	2.77%	12.88	3.51%

time with a maximum prediction horizon size of 35s, and the optimal control signal can be obtained and sent to relevant controllers within 1 second.

3. The vehicle with OSIP outperforms the system without it in energy saving at all initial battery SoC level, and it has more potential in fuel saving when initial battery SoC is high.

4. The proposed energy management method is robust and reliable for energy saving in all pushback driving cycles, and up to 17% fuel and 13% total energy loss can be saved via the proposed cyber-physical control.

In future work, the proposed algorithm will be implemented in a real connected hybrid aircraft-towing tractor for further verification in road test. The proposed online swarm intelligent optimization method will be integrated with an artificial neural network and reinforcement learning for more advanced control scenario including the platoon and fleet control.

ACKNOWLEDGEMENT

The work is funded by Innovate UK (Grant 102253). The authors gratefully acknowledge the support from Textron Ground Support Equipment UK and Hyper-Drive Innovation.

REFERENCE

[1] B. Sampathnarayanan, L. Serrao, S. Onori, G. Rizzoni, S. Yurkovich, and Asme, "Model Predictive Control As an Energy Management Strategy for Hybrid Electric Vehicles," Proc. Asme Dyn. Syst. Control Conf. 2009, Pts a B, pp. 1161–1168, Jan. 2010.

[2] X. Hu, N. Murgovski, L. Johannesson, and B. Egardt, "Energy efficiency analysis of a series plug-in hybrid electric bus with different energy management strategies and battery sizes," *Appl. Energy*, vol. 111, pp. 1001–1009, 2013.

[3] C. Lv, J. Zhang, Y. Li, and Y. Yuan, "Mechanism analysis and evaluation methodology of regenerative braking contribution to energy efficiency improvement of electrified vehicles," *Energy Convers. Manag.*, vol. 92, pp. 469–482, 2015.

[4] Q. Zhou, G. Tan, X. Guo, Z. Fang, and B. Gong, "Relationship between braking force and pedal force of a pedal controlled parallelized energy-recuperation retarder system," *SAE Tech. Pap.*, Apr. 2014.

[5] B. Wang, X. Huang, J. Wang, X. Guo, and X. Zhu, "A robust wheel slip ratio control design combining hydraulic and regenerative braking systems for in-wheel-motors-driven electric Vehicles," *J. Franklin Inst.*, vol. 352, no. 2, pp. 577–602, Feb. 2015.

[6] C. Lv *et al.*, "Simultaneous Observation of Hybrid States for Cyber-Physical Systems : A Case Study of Electric Vehicle Powertrain," *IEEE Trans. Cybern.*, vol. in press, pp. 1–11, 2017.

[7] Q. Zhou, X. Guo, G. Tan, X. Shen, Y. Ye, and Z. Wang, "Parameter Analysis on Torque Stabilization for the Eddy Current Brake: A Developed Model, Simulation, and Sensitive Analysis," *Math. Probl. Eng.*, vol. 2015, pp. 1–10, 2015.

[8] J. Peng, H. He, and R. Xiong, "Rule based energy management strategy for a series–parallel plug-in hybrid electric bus optimized by dynamic programming," *Appl. Energy*, vol. 185, pp. 1633–1643, Jan. 2016.

[9] J. Peng, H. Fan, H. He, and D. Pan, "A Rule-Based Energy Management Strategy for a Plug-in Hybrid School Bus Based on a Controller Area Network Bus," *Energies*, vol. 8, no. 12, pp. 5122–5142, Jun. 2015.

[10] C. Lv *et al.*, "Cyber-Physical System Based Optimization Framework for Intelligent Powertrain Control," *SAE Int. J. Commer. Veh.*, vol. 10, no. 1, pp. 2017-01–0426, 2017.

[11] X. Hu, H. Wang, and X. Tang, "Cyber-Physical Control for Energy-Saving Vehicle Following with Connectivity," *IEEE Trans. Ind. Electron.*, vol. 46, no. c, pp. 1–1, 2017.

[12] W. Wu, Z. Yang, and K. Li, "Internet of Vehicles and applications," in *Internet of Things：Priciples and Paradigms*, B. Rajkumar and V. Amir Dastjerdi, Eds. Elsevier, 2016, pp. 299–317.

[13] S. Xu, S. E. Li, K. Deng, S. Li, S. Member, and B. Cheng, "A Unified Pseudospectral Computational Framework for Optimal Control of Road Vehicles," *IEEE/ASME Trans. MECHATRONICS*, vol. 20, no. 4, pp. 1499–1510, 2015.

[14] Y. Huang, H. Wang, A. Khajepour, H. He, and J. Ji, "Model predictive control power management strategies for HEVs: A review," *J. Power Sources*, vol. 341, pp. 91–106, 2017.

[15] S. Zhang, R. Xiong, and F. Sun, "Model predictive control for power management in a plug-in hybrid electric vehicle with a hybrid energy storage system," *Applied Energy*, vol. 185, Elsevier Ltd, pp. 1654–1662, 2015.

[16] H. Borhan, A. Vahidi, A. M. Phillips, M. L. Kuang, I. V. Kolmanovsky, and S. Di Cairano, “MPC-based energy management of a power-split hybrid electric vehicle,” *IEEE Trans. Control Syst. Technol.*, vol. 20, no. 3, pp. 593–603, May 2012.
[17] Y. Zhang, G. Lu, H. Xu, and Z. Li, “Tuneable model predictive control of a turbocharged diesel engine with dual loop exhaust gas recirculation,” *Proc. Inst. Mech. Eng. Part D J. Automob. Eng.*, Oct. 2017.
[18] F. Yan, J. Wang, and K. Huang, “Hybrid Electric Vehicle Model Predictive Control Torque-Split Strategy Incorporating Engine Transient Characteristics,” *IEEE Trans. Veh. Technol.*, vol. 61, no. 6, pp. 2458–2467, Jul. 2012.
[19] G. Ripaccioli, A. Bemporad, F. Assadian, and C. Dextreit, “Hybrid Modeling , Identification , and Predictive Control : An Application to Hybrid Electric Vehicle Energy Management,” in *Hybrid Systems: Computation and Control*, 2009, pp. 321–335.
[20] T. C. J. Romijn, M. C. F. Donkers, J. T. B. . Kessels, and S. Weiland, “Receding Horizon Control for Distributed Energy Management of a Hybrid Heavy-Duty Vehicle with Auxiliaries,” *IFAC-PapersOnLine*, vol. 48, no. 15, pp. 203–208, 2015.
[21] Y. Huang, A. Khajepour, F. Bagheri, and M. Bahrami, “Modelling and optimal energy-saving control of automotive air-conditioning and refrigeration systems,” *Proc. Inst. Mech. Eng. Part D J. Automob. Eng.*, vol. 231, no. 3, pp. 291–309, Feb. 2017.
[22] F. Xu, H. Chen, X. Gong, and Q. Mei, “Fast nonlinear model predictive control on FPGA using particle swarm optimization,” *IEEE Trans. Ind. Electron.*, vol. 63, no. 1, pp. 310–321, Jan. 2016.
[23] S.-Y. Chen, Y.-H. Hung, C.-H. Wu, and S.-T. Huang, “Optimal energy management of a hybrid electric powertrain system using improved particle swarm optimization,” *Appl. Energy*, vol. 160, pp. 132–145, 2015.
[24] A. Ostadi and M. Kazerani, “A Comparative Analysis of Optimal Sizing of Battery-Only, Ultracapacitor-Only, and Battery-Ultracapacitor Hybrid Energy Storage Systems for a City Bus,” *IEEE Trans. Veh. Technol.*, vol. 64, no. 10, pp. 4449–4460, Oct. 2015.
[25] S. Ebbesen, C. Dönitz, and L. Guzzella, “Particle swarm optimisation for hybrid electric drive-train sizing,” *Int. J. Veh. Des.*, vol. 58, no. 2/3/4, p. 181, 2012.
[26] M. Pourabdollah, E. Silvas, N. Murgovski, M. Steinbuch, and B. Egardt, “Optimal sizing of a series PHEV: Comparison between convex optimization and particle swarm optimization,” in *IFAC-PapersOnLine*, 2015, vol. 28, no. 15, pp. 16–22.
[27] A. H. Gandomi, G. J. Yun, X. S. Yang, and S. Talatahari, “Chaos-enhanced accelerated particle swarm optimization,” *Commun. Nonlinear Sci. Numer. Simul.*, vol. 18, no. 2, pp. 327–340, 2013.
[28] Q. Zhou, W. Zhang, S. Cash, O. Olatunbosun, H. Xu, and G. Lu, “Intelligent sizing of a series hybrid electric power-train system based on Chaos-enhanced accelerated particle swarm optimization,” *Appl. Energy*, vol. 189, pp. 588–601, 2017.
[29] N. Murgovski, L. Johannesson, J. Sjöberg, and B. Egardt, “Component Sizing of a Plug-in Hybrid Electric Powertrain via Convex Optimization,” *Mechatronics*, vol. 22, no. 1, pp. 106–120, 2012.
[30] M. Chen and G. A. Rincón-Mora, “Accurate electrical battery model capable of predicting runtime and I-V performance,” *IEEE Trans. Energy Convers.*, vol. 21, no. 2, pp. 504–511, Jun. 2006.
[31] Z. Chen, R. Xiong, C. Wang, and J. Cao, “An on-line predictive energy management strategy for plug-in hybrid electric vehicles to counter the uncertain prediction of the driving cycle,” *Appl. Energy*, vol. 185, pp. 1633–1672, 2017.
[32] H. Borhan, A. Vahidi, A. M. Phillips, M. L. Kuang, I. V. Kolmanovsky, and S. Di Cairano, “MPC-Based Energy Management of a Power-Split Hybrid Electric Vehicle,” *IEEE Trans. Control Syst. Technol.*, vol. 20, no. 3, pp. 593–603, May 2012.
[33] S. G. Li, S. M. Sharkh, F. C. Walsh, and C. N. Zhang, “Energy and Battery Management of a Plug-In Series Hybrid Electric Vehicle Using Fuzzy Logic,” *IEEE Trans. Veh. Technol.*, vol. 60, no. 8, pp. 3571–3585, 2011.
[34] “ETAS products,” *ETAS group*, 2017. [Online]. Available: https://www.etas.com/en/index.php?langS=true.
[35] S. Cash and O. Olatunbosun, “Fuzzy logic field-oriented control of an induction motor and a permanent magnet synchronous motor for hybrid / electric vehicle traction applications,” vol. 9, no. 3, 2017.
[36] Rachel Cooper, “New hybrid aircraft push-back tractor on show at Inter Airport Europe Exhibition,” *Hyperdrive Innovation Limited*, 2017. [Online]. Available: https://hyperdriveinnovation.com/new-hybrid-aircraft-push-back-tractor-on-show-at-inter-airport-europe-exhibition/.